ADVANCED FUNCTIONAL MATERIALS
www.afm-journal.de



# Soft Core/Shell Packages for Stretchable Electronics

*Chi Hwan Lee, Yinji Ma, Kyung-In Jang, Anthony Banks, Taisong Pan, Xue Feng, Jae Soon Kim, Daeshik Kang, Milan S. Raj, Bryan L. McGrane, Briana Morey, Xianyan Wang, Roozbeh Ghaffari, Yonggang Huang,* and John A. Rogers**

**This paper presents materials and core/shell architectures that provide optimized mechanical properties in packages for stretchable electronic systems. Detailed experimental and theoretical studies quantitatively connect the geometries and elastic properties of the constituent materials to the overall mechanical responses of the integrated systems, with a focus on interfacial stresses, effective modulus, and maximum extent of elongation. Specific results include core/shell designs that lead to peak values of the shear and normal stresses on the skin that remain less than 10 kPa even for applied strains of up to 20%, thereby inducing minimal somatosensory perception of the device on the human skin. Additional, strain-limiting mesh structures embedded in the shell improve mechanical robustness by protecting the active components from strains that would otherwise exceed the fracture point. Demonstrations in precommercial stretchable electronic systems illustrate the utility of these concepts.**

## 1. Introduction

Advances in stretchable electronics enable soft, conformal integration of high performance semiconductor devices onto various internal and external surfaces of the human body. These mechanical features result in highly functional abiotic/biotic interfaces with the potential for diverse applications in healthcare.[1–4] For mounting on the skin, desirable physical attributes include low elastic modulus and reversible response to large strain deformations (up to ≈30%), in formats that minimize the stresses that develop at the interface with the skin. These properties not only facilitate robust bonding, but also reduce any mechanical sensation associated with coupling of the device to the skin.[5] Recent work[1] demonstrates that such characteristics can be achieved at the system level, even with hard, commercially available electronic chips, by exploiting microfluidic spaces that decouple the mechanics of the constituent devices and associated interconnect networks from the supporting elastomeric substrate and encapsulation layer. A disadvantage of this construct arises from the possibility of fluid leakage. In the present paper, we demonstrate the extent to which replacement of the fluid in this type

Dr. C. H. Lee, Dr. K.-I. Jang, A. Banks, Dr. D. Kang
Department of Materials Science and Engineering
and Frederick Seitz Materials Research Laboratory
University of Illinois at Urbana-Champaign
Urbana, IL 61801, USA

Dr. Y. Ma, T. Pan
Department of Civil and Environmental Engineering
and Mechanical Engineer
Center for Engineering and Health and Skin Disease Research Center
Northwestern University
Evanston, IL 60208, USA

Dr. Y. Ma, Prof. X. Feng
Department of Engineering Mechanics
Center for Mechanics and Materials
Tsinghua University
Beijing 100084, China

T. Pan
State Key Laboratory of Electronic Thin Films and Integrated Devices
University of Electronic Science and Technology of China
Chengdu, Sichuan 610054, China

J. S. Kim
Department of Chemistry
University of Illinois at Urbana-Champaign
Urbana, IL 61801, USA

M. S. Raj, B. L. McGrane, B. Morey, Dr. X. Wang,
Dr. R. Ghaffari
MC10, Inc.
Cambridge, MA 02140, USA

Prof. Y. Huang
Department of Civil and Environmental Engineering
and Mechanical Engineering
Northwestern University
Evanston, IL 60208, USA
E-mail: y-huang@northwestern.edu

Prof. J. A. Rogers
Department of Materials Science and Engineering
Chemistry, Mechanical Science and Engineering
Electrical and Computer Engineering
Beckman Institute for Advanced Science and Technology
and Frederick Seitz Materials
Research Laboratory
University of Illinois at Urbana-Champaign
Urbana, IL 61801, USA
E-mail: jrogers@illinois.edu

DOI: 10.1002/adfm.201501086

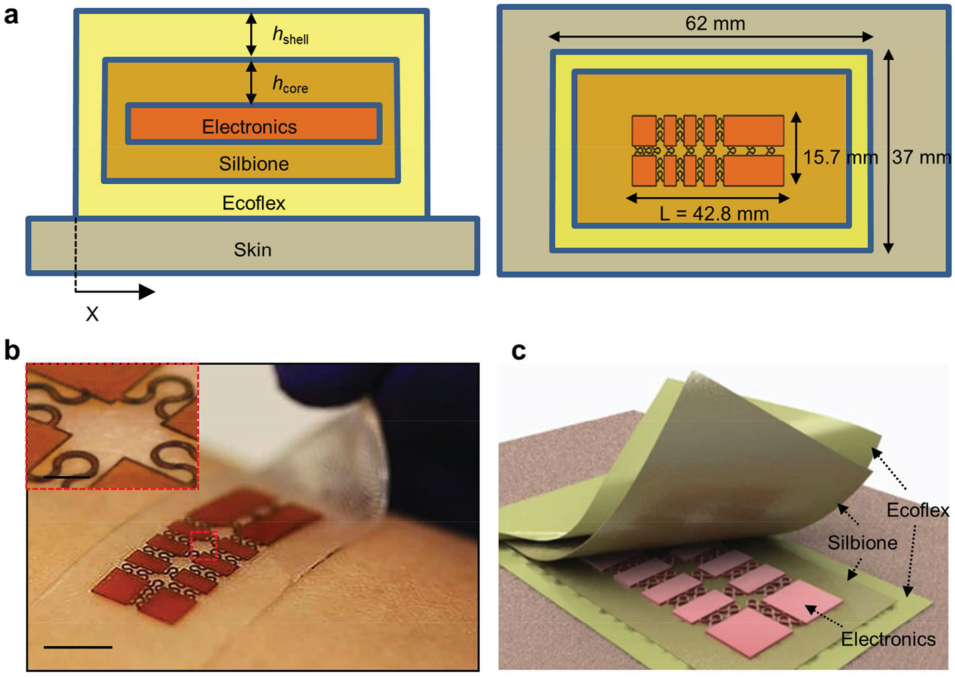


**Figure 1.** a) Cross-sectional and top view illustrations of representative layers in a core/shell structure with embedded stretchable electronics. b) Optical images (scale bar, 5 mm; inset scale bar: 1 mm). c) A schematic illustration of a representative system with a peel-away view at one of the corners.

of core/shell structure with an ultralow modulus solid elastomer can capture the favorable mechanics while simultaneously eliminating any possibility for leakage. Experimental and theoretical studies reveal the important features of the underlying materials and mechanics aspects and their dependence on key design variables. The results not only demonstrate effective core/shell designs, but also establish general design rules with broad implications for the field of stretchable electronics.

## 2. Results and Discussion

**Figure 1**a presents a schematic cross-sectional illustration of the core/shell design with a thin, stretchable electronic system located at the midpoint. The electronics include device islands joined together by serpentine interconnects. A sheet of polyimide (60 μm thickness, Young's modulus ($E$) = 2.5 GPa) geometrically configured using a laser system (LMT-5000s Dual Laser System, Potomac, USA) into the dimensions of the electronics serves as a simple test vehicle in the studies of the mechanics. Details are in Figure S1 in the Supporting Information. A fully functional, wireless system with similar layout, integrated in an optimized core/shell construct, appears at the end. The key feature of the layout of Figure 1a is that electronics reside in an ultralow-modulus elastomer (core) to provide mechanical isolation from the surroundings. A thin enclosure formed using a different elastomer (shell) provides a robust, mechanically tough interface for handling and lamination onto the skin. This layout captures some of the mechanical advantages of recently reported microfluidic packaging schemes but without the need for hermetic sealing.[1] The structure reported here uses a silicone elastomer (Silbione RT Gel 4717 A/B, Bluestar Silicone, USA, $E = 5$ kPa, thickness $h_{core}$ in Figure 1a) for the core and a thin layer of silicone with a modified formulation (Ecoflex, Smooth-On, Easton, Pennsylvania, $E$ = 60 kPa, thickness $h_{shell}$ in Figure 1a) for the shell. Figure 1b,c presents an optical image and a schematic illustration in a peel-away view at one of the corners. The system can softly integrate onto the epidermis in a manner that minimizes interfacial stresses and mechanical constraints on natural body motions and, at the same time, enables application and removal without damage to the device or the skin. Additional strain-limiting mesh structures can be embedded in the shell to improve the mechanical robustness, as described subsequently.

The extremely low effective tensile modulus of this system represents an important characteristic. **Figure 2**a shows the stress–strain curves of the core/shell package ($h_{core}$ = 500 μm and $h_{shell}$ = 5 μm), with and without the electronics (here, the polyimide mechanical test structure), obtained from dynamic mechanical analysis (DMA, TA instruments, Q800) and finite element analysis (FEA). The experimental (DMA) and computational (FEA) results agree well without any parameter fitting. Here, the force is applied to regions at opposite ends of the core/shell package. The stress (shown in logarithmic scale) is the ratio of force to the net cross sectional area of the core/shell package, and the strain is the percentage elongation of the electronic portion of the system, given by $\varepsilon = \Delta L/L$, where $L$ is initial length (Figure 1a) and $\Delta L$ is the change due to stretching. The effective tensile moduli obtained from Figure 2a are ≈22 and ≈5 kPa for the package with and without electronics, respectively. Both values are far smaller than the modulus of the skin (≈130 kPa),[5] suggesting that the system will impose minimal mechanical constraints on the motion of the skin. For comparison, Figure 2a also shows the results for the same electronics

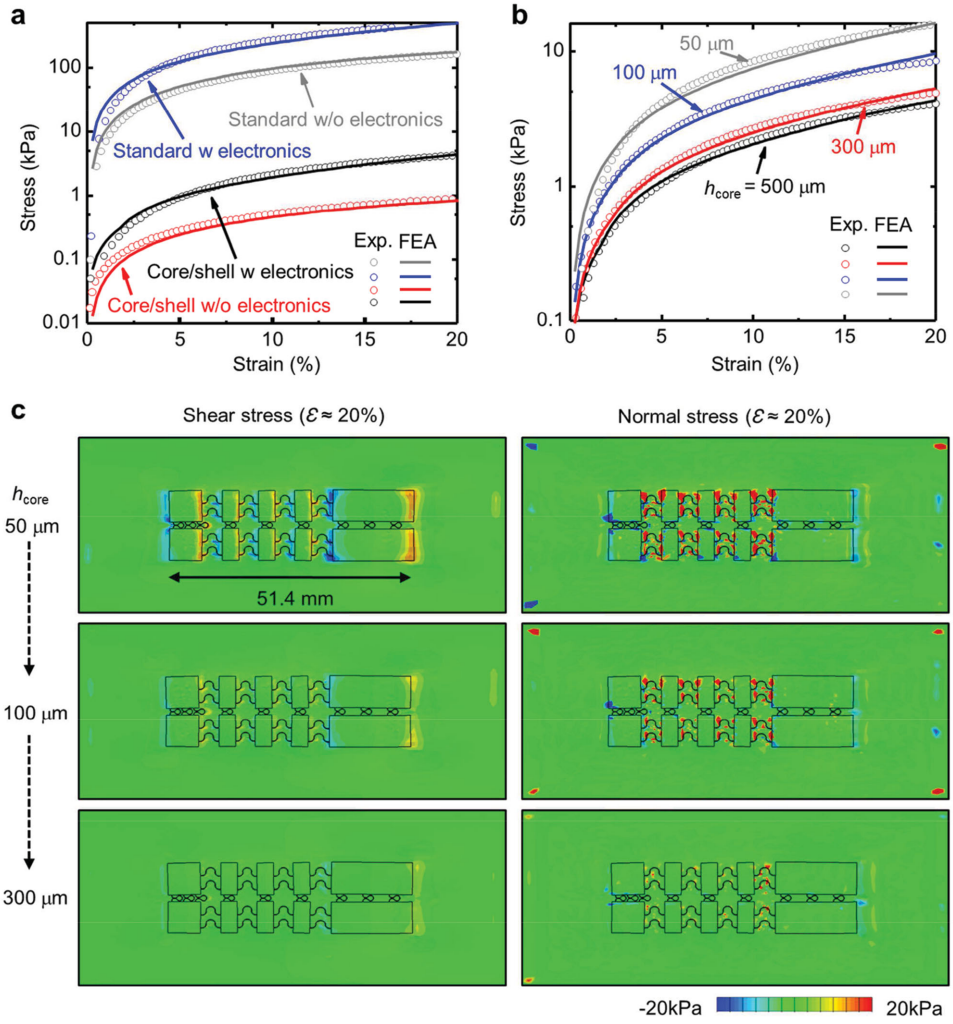


**Figure 2.** a) Experimental and finite element analysis (FEA) results of the stress–strain relationship (in logarithmic scale) for core/shell structures and standard packages with and without electronics. b) Experimental and FEA results of stress–strain responses (in logarithmic scale) of the core/shell structure with the electronics (without the skin) with different $h_{core}$ from 50 to 500 μm. c) FEA results of shear (left) and normal (right) stress distributions at the interface with the skin for normal skin sensitivity (20 kPa) at 20% strain with different $h_{core}$ from 50 to 300 μm.

but encapsulated above and below with a standard elastomer used in stretchable electronics (Sylgard 184, $E$ = 1 MPa, total thickness = ≈1 mm). The effective tensile moduli in this case, with and without the electronics, are 2.8 and 1 MPa, respectively. These values are more than 120 times larger than those for the core/shell design, and they are more than ten times larger than that of the skin. Significant differences also exist in the degree of stretchability. Assuming a 3% yield strain for the polyimide, the elastic stretchabilities of systems with the core/shell and standard packages are 22% and 5%, respectively. Representative strain distributions for the core/shell structure at $\varepsilon$ = 22% and the standard package at $\varepsilon$ = 5% appear in Figure S2 (Supporting Information).

The value of $h_{core}$ is critically important due to its role in mechanical isolation, i.e., so-called strain isolation,[6–8] of the electronics. Figure 2b presents experimental (DMA) and computational (FEA) results of uniaxial stress–strain responses for different values of $h_{core}$, with all other parameters fixed ($h_{shell}$ = 5 μm), and clamping in the same configuration as results for Figure 2a. As with the other results, these experimentally obtained stress–strain curves agree well with FEA without any parameter fitting. The effective tensile modulus of the core/shell package decreases as the $h_{core}$ increases, and approaches an asymptotic value for large $h_{core}$ (>≈300 μm).

Actual use involves lamination of the devices on the surface of the skin. Here, the stresses that develop at the interface during deformation of the skin are important because they can drive delamination and they determine the somatosensory perception of the presence of the device. Figure 2c shows the shear (left) and normal (right) stress distributions at the interface obtained by FEA for the case of $h_{core}$ = 50–300 μm and $h_{shell}$ = 5 μm with a device laminated onto a phantom skin substrate (Ecoflex, 2 mm thickness, $E$ = 60 kPa). The shear and normal stresses with $h_{core}$ = 50 and 100 μm show many regions that exceed the threshold for somatosensory perception of forces by normal skin (20 kPa),[5] whereas those for $h_{core}$ = 300 μm are below threshold at almost all locations. Additional plots for the case of heightened skin sensitivity (≈2 kPa)[9,10] appear in

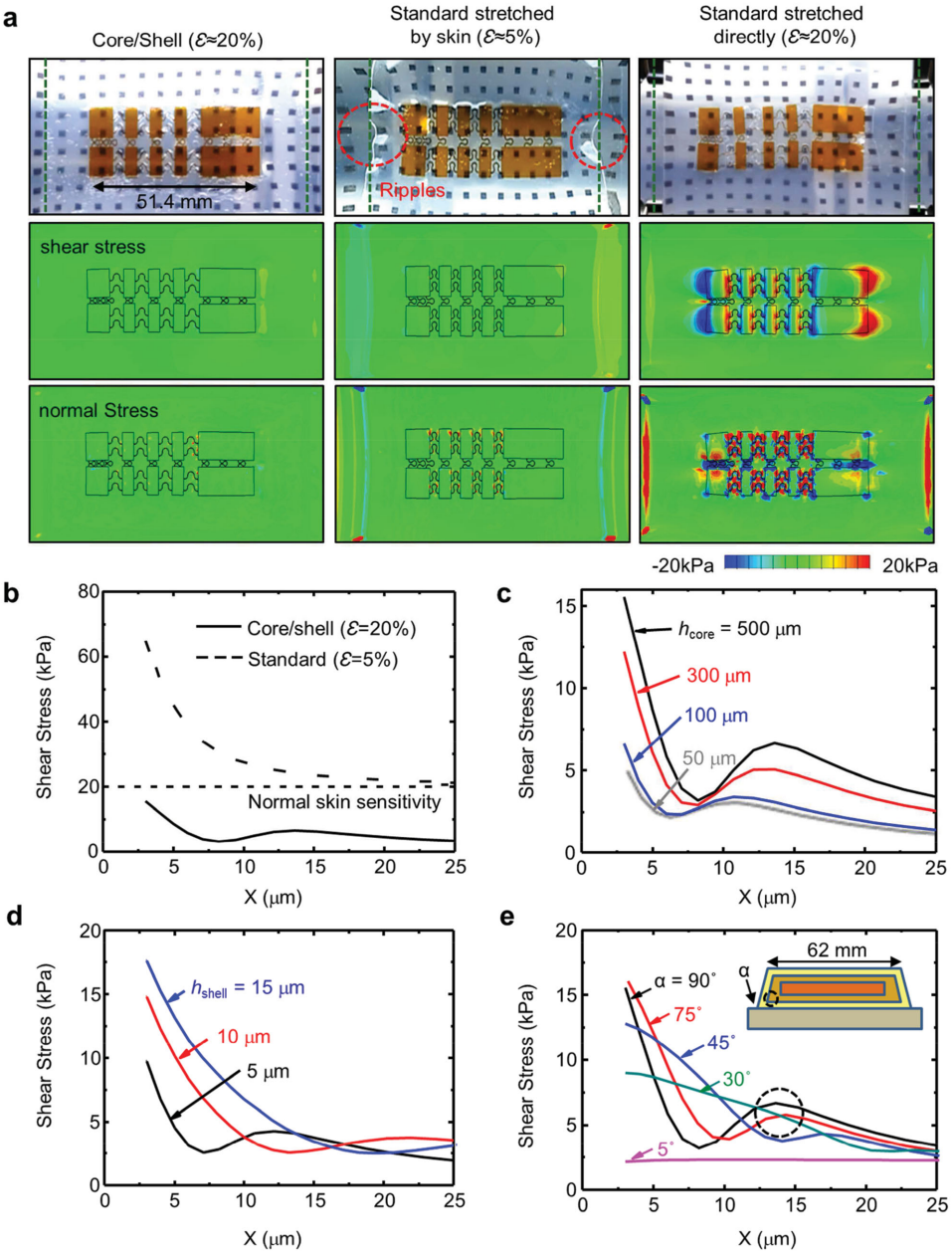


**Figure 3.** a) Optical images and FEA results of shear and normal stress distributions at the interface with the skin for the core/shell structure at 20% strain (left), the standard package stretched by the skin at 5% strain (middle), and the standard package stretched directly at 20% strain (right). b) FEA results of shear stress concentration near the edge for the core/shell structure at 20% strain and the standard package at 5% strain. c) FEA results of shear stress concentration near the edge at 20% strain with different $h_{core}$ from 50 to 500 μm. d) FEA results of shear stress concentration near the edge at 20% strain with different $h_{shell}$ from 5 to 15 μm. e) FEA results of shear stress concentration near the edge with different tapered angles ($\alpha$ = 5°, 30°, 45°, 75°, 90°). The inset shows a cross-sectional illustration of the core/shell structure with electronics and a taper angle of $\alpha$.

Figure S3 (Supporting Information). The results clearly show that the stresses on the skin decrease as $h_{core}$ increases. Varying $h_{shell}$ has no significant effects because, for the range studied, $h_{shell}$ is much smaller than $h_{core}$. Results are summarized in Figures S4 and S5 (Supporting Information) for normal and heightened skin sensitivities.

**Figure 3**a (left column) presents optical images of a device and computed stress distributions for phantom skin (Ecoflex, 2 mm thickness, patterned with a square array of fiducial markers on the backside to highlight the deformations) with $h_{core}$ = 500 μm and $h_{shell}$ = 5 μm, for $\varepsilon$ = 20%. Here, the force is applied to regions at opposite ends of the skin. The green dashed lines highlight the outer boundary of the package. The length of the electronics region increases from an original value of 42.8 mm to 51.4 mm (Figure 3a, left column). Results for stretching in the orthogonal direction appear in Figure S6 (Supporting Information). The deformation in the phantom skin shows little constraint in motion associated with the

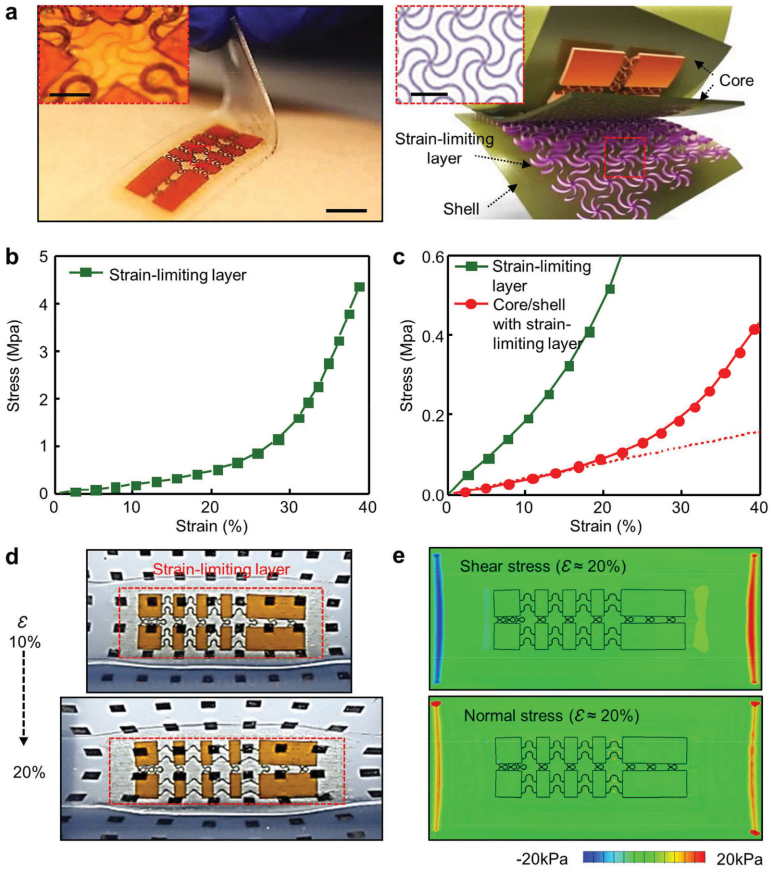


**Figure 4.** a) Optical images (scale bar, 5 mm; inset scale bar, 1 mm) and an exploded view schematic illustration (inset scale bar, 100 μm) of a core/shell structure with electronics that includes a strain-limiting layer in the form of a lithographically defined wave filamentary network of polyimide (insets). b,c) Experimental results for the strain–stress response of a strain-limiting layer only and of the core/shell structure with the strain-limiting layer. d,e) Optical images of the system and FEA results of shear and normal stress distribution of the phantom skin for the core/shell package with strain-limiting layer at 20% strain.

electronics, as illustrated by the uniform separations between the fiducial dots. The FEA results indicate that the shear and normal stresses on the skin are less than ≈10 kPa, i.e., below the threshold for sensation of normal skin. Results for the standard package (Sylgard 184, $E$ = 1 MPa, total thickness = ≈1 mm) appear in Figure 3a (middle and right columns). Here, both edges ripple and delaminate (red dashed circles in Figure 3a, middle column) for $\varepsilon$ larger than ≈5%. In fact, this system is sufficiently stiff that the standard package must be stretched directly (as opposed to stretching by application of forces to the phantom skin in Figure 3a, left column) to reach 20% strain (Figure 3a, right column). Here, the corresponding shear and normal stresses of the surface of the skin are substantially higher than the threshold for sensation (20 kPa), with peak values that reach ≈100 kPa.

As indicated in the image in the center of Figure 3a, delamination tends to initiate from the edges, at points of stress concentrations. Figure 3b confirms that these stresses evaluated across a 25 μm wide boundary zone around the edge of the core/shell structure are much lower than those of the standard package. For the former, the values lie below the threshold for normal skin sensitivity (20 kPa), even at $\varepsilon$ = 20%. By contrast, even at 5% strain, the stress concentrations for the standard package reach ≈60 kPa and are responsible for the delamination and ripples apparent in Figure 3a (middle column). The edge stresses for the core/shell structure can be reduced even further by decreasing $h_{core}$ or $h_{shell}$ (Figure 3c,d). Reducing $h_{core}$ increases, however, stresses in the central regions of the skin, as discussed in Figures 2c and S3 (Supporting Information). As a result, $h_{core}$ must be selected to balance the stresses on the skin beneath the electronics (Figure 2c, for normal skin sensitivity) and the stress concentrations at the edges (Figure 3c, to prevent delamination). Tapering the thickness of the perimeter boundary of the core/shell structure provides an alternative means to decrease the edge stresses in a manner that does not affect the central regions of the skin. Figure 3e presents calculated (FEA) stress distributions at the edge for a representative core/shell structure ($h_{core}$ = 500 μm, $h_{shell}$ = 5 μm, and a length evaluated at the top of the package of 62 mm as shown in Figure 3e, inset) under uniaxial stretching of the skin with $\varepsilon$ = 20% for different taper angles ($\alpha$ = 5°, 30°, 45°, 75°, 90°). For all cases, the stresses display maximum values at the edge, with local maxima (dashed circle in Figure 3e) observable for large angles near the inside corner of the core (marked by the circle in the inset image). As expected, the edge stresses decrease with taper angle, thereby reducing the propensity for edge-initiated delamination. The corresponding normal stresses for Figure 3b–e appear in Figure S7 (Supporting Information).

The soft, low modulus mechanical properties enabled by the strain-isolating core material are key features of the design. An associated disadvantage is in an increased potential for inadvertent stretching of the electronics beyond the fracture limits. The addition of a layer with a strongly nonlinear stress–strain relationship can eliminate this disadvantage by offering a low modulus response at small strains and high modulus response to counter the effects of large strains.[11] This layer can take the form of an engineered open mesh fabric, as described recently.[11] **Figure 4**a presents an optical image (left) and an exploded schematic illustration (right) of a core/shell structure that incorporates such a strain-limiting mesh constructed in polyimide (60 μm thick, $E$ = 2.5 GPa). This network consists of a uniform triangular lattice of repeating, filamentary building block units with horseshoe geometries (Figure 4a, insets).[11] Tensile loads cause these networks to unfurl, straighten, and stretch in a manner that imparts a low modulus response for strains less than ≈20% and a sharp transition to a high modulus regime for strains larger than ≈40% (Figure 4b). Figure 4c shows results of uniaxial testing that reveal a slowly increasing local slope (tangential modulus) of the stress–strain curve at low strains (<20%) where bending motions dominate the deformation of the network, followed by rapid increase at high strains

(>30%) where stretching of the horseshoe shapes causes the filaments to begin to reach full extension such that the material itself, rather than the motions of the filaments, dominates the response. Figure 4d presents optical images of a system with this type of strain-limiting layer, mounted on the phantom skin as with results of Figure 3a, for uniaxial stretching at opposite ends of the skin to $\varepsilon = 10\%$ and 20%. The nonuniform deformations in the skin at high strains (>20%) illustrate that the resulting mechanics associated with the strain-limiting layer leads to reductions in the levels of strain in this region upon overall stretching of the skin. The FEA results in Figure 4e confirm that the stresses at the skin surface for $\varepsilon \approx 20\%$ remain within the normal human skin sensitivity (20 kPa). The stress distributions with and without the strain-limiting layer plotted over a scale that corresponds to heightened skin sensitivity (2 kPa) appear in Figure S8 (Supporting Information).

This core/shell concept is compatible with emerging commercial classes of stretchable electronic systems. An example exploits a wearable device (MC10, USA) equipped with tri-axis accelerometers, temperature sensors, a Bluetooth low-energy communication system, and a battery, all connected in an island/serpentine geometry. **Figure 5**a presents this system in a core/shell structure (left image, $h_{core} = 1$ mm, $h_{shell} = 5$ μm) and in a standard package (right image, Sylgard 184, total thickness ≈ 2 mm), laminated on the wrist. The device in the core/shell structure can intimately integrate onto the epidermis without delaminations throughout the natural range of motions of the wrist. By contrast, the device in the standard package tends to easily delaminate from the edge. This behavior arises from the low effective tensile modulus for the core/shell case (40 kPa), i.e., ≈70 times smaller than that for the standard package (2.8 MPa), confirmed by the experimental and computational (FEA) stress–strain measurements (Figure 5b). The enabled functionality allows wireless, real-time monitoring of accelerations and temperature during vigorous exercise (i.e., dumbbell lifting) as illustrated in Figure S9 (Supporting Information). The results in this simple demonstration indicate that the body temperature rises quickly, by ≈1.5 °C, during lifting (10 lb weight, seven times for ≈35 s) followed by a slow decrease during a subsequent resting state (Figure 5c), along with the visualized arm motions from the measured accelerations in *x*, *y*, and *z*-axis (Figure 5d).

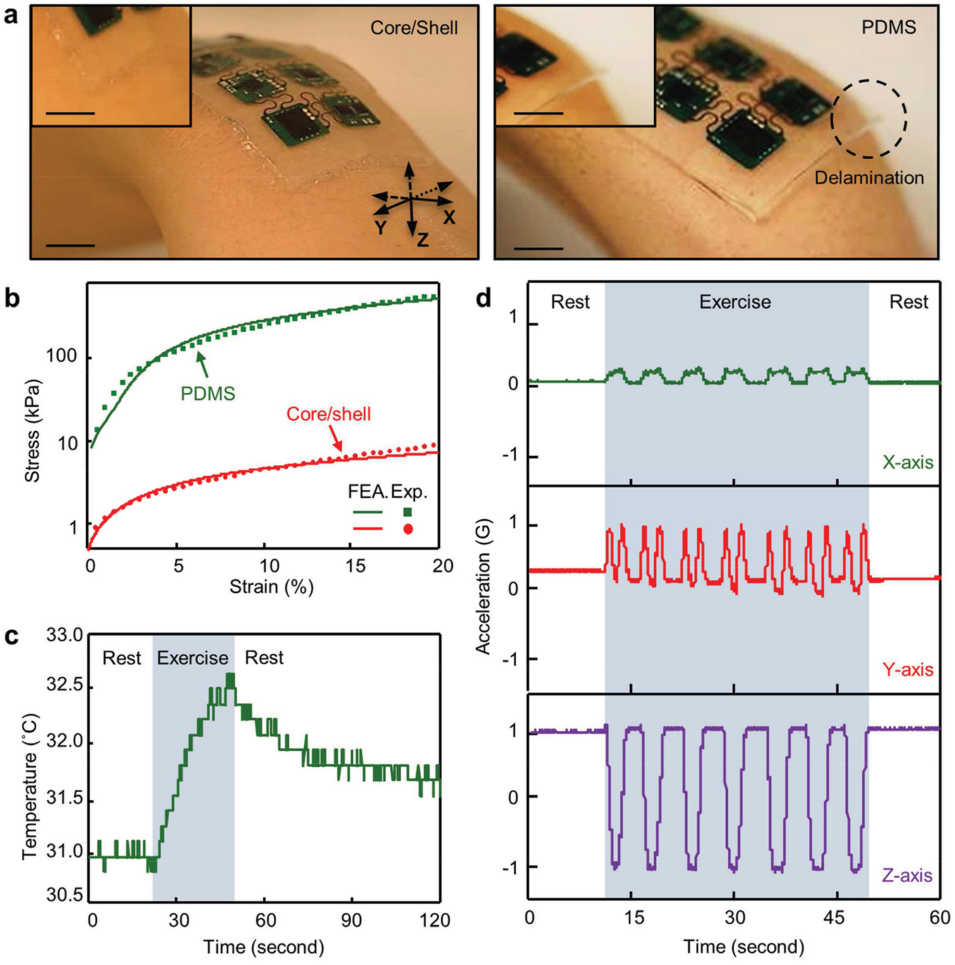


**Figure 5.** a) Optical images (scale bar, 1 cm) for a core/shell structure (left) and a standard package (right) with commercially available wireless electronics (MC10, USA), laminated on the wrist. Insets (scale bar, 1 cm) show enlarged images near the edges. b) Experimental and FEA results of stress–strain responses (in logarithmic scale) for these systems, with the electronics. c) Real-time monitoring of temperature changes during the exercise (10 lb dumbbell lifting, seven times for ≈35 s) and in a resting condition. d) The corresponding changes in accelerations in *x*, *y* and *z*-axis.

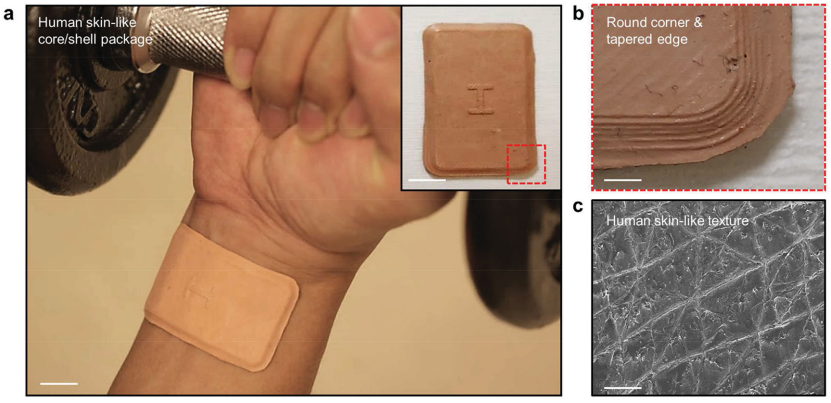


**Figure 6.** a) Optical image (scale bar, 1 cm) of core/shell package applied on the wrist during dumbbell lifting. The inset (scale bar, 1 cm) shows an image of the core/shell structure only. A patterned campus logo "I" for the University of Illinois at Urbana-Champaign appears in the middle of the surface. b) Enlarged image (scale bar, 5 mm) at a corner of the core/shell structure to highlight the rounded corner and tapered edge. c) SEM image (scale bar, 0.5 mm) of the human skin-like textured surface.

Human skin-like colors, textures, and other features can readily be incorporated to modulate the physical appearance and aesthetics of the system. **Figure 6**a shows an example obtained with a commercially available pigment (Slic Pig, Flesh tone silicone pigment, Smooth-On, Inc.). The design layout consists of round corners and tapered edges ($\alpha \approx 30°$) to minimize the edge stresses for the core/shell package, thereby hindering delamination (Figure 6b). The human skin-like surface texturing on the surface of core/shell package results from use of a mould that offers skin-like texture (see the Experimental Section for the details). A representative scanning electron microscopy (SEM) image of the textured surface of the core/shell package appears in Figure 6c.

## 3. Conclusion

The soft core/shell concepts introduced here provide simple, straightforward means to enhance the properties of stretchable electronic devices by minimizing interface stresses and mechanical constraints on natural motions and by improving the overall stretchability. These characteristics are particularly important in applications that involve soft, intimate integration onto the epidermis with minimal somatosensory perception of the device. Experimental and theoretical results provide insights into the observed behaviors and opportunities to achieve skin-coupled electronic systems that are mechanically imperceptible to the wearer.

## 4. Experimental Section

*Finite Element Analysis (FEA)*: ABAQUS commercial software[12] was used to study the mechanics response of core/shell package and standard package. Silbione, Ecoflex, and Sylgard 184 were modeled by the hexahedron element (C3D8R), while the electronics and strain-limiting layer were modeled by the composite shell element (S4R).

*Preparation of Artificial Skin Mould*: A mixture of commercially available materials was used for preparing the artificial skin sample; Dragon Skin (Dragon Skin 30, Smooth-On, Inc.) and Slic Pig (Slic Pig, Flesh tone silicone pigment, Smooth-On, Inc.). The Dragon Skin (1:1 ratio by weight of part A and part B) was mixed with Slic Pig (3% by weight) and then applied on the forearm, followed by curing at room temperature for ≈1 h. Peeling the fully cured artificial skin completed the process where the textured surface allowed it to be used as a mould (Figure S10, Supporting Information).

## Supporting Information

Supporting Information is available from the Wiley Online Library or from the author.

## Acknowledgements

This work was supported by DOE-BES under Grant No. DE-FG02-07ER46471 administered through the Frederick Seitz Materials Research Laboratory. X.F. and Y.M. acknowledge the support from the National Basic Research Program of China (Grant No. 2015CB351900) and National Natural Science Foundation of China (Grant Nos. 11402135, 11320101001). C.H.L., Y.M., and K.-I.J. contributed equally to this work.

Received: March 18, 2015
Published online: May 15, 2015

[1] S. Xu, Y. Zhang, L. Jia, K. E. Mathewson, K.-I. Jang, J. Kim, H. Fu, X. Huang, P. Chava, R. Wang, S. Bhole, L. Wang, Y. J. Na, Y. Guan, M. Flavin, Z. Han, Y. Huang, J. A. Rogers, *Science* **2014**, *344*, 70.
[2] D.-H. Kim, N. Lu, R. Ma, Y.-S. Kim, R.-H. Kim, S. Wang, J. Wu, S. M. Won, H. Tao, A. Islam, K. J. Yu, T.-I. Kim, R. Chowdhury, M. Ying, L. Xu, M. Li, H.-J. Chung, H. Keum, M. McCormick, P. Liu, Y.-W. Zhang, F. G. Omenetto, Y. Huang, T. Coleman, J. A. Rogers, *Science* **2011**, *333*, 838.
[3] J.-W. Jeong, M. K. Kim, H. Cheng, W.-H. Yeo, X. Huang, Y. Liu, Y. Zhang, Y. Huang, J. A. Rogers, *Adv. Healthcare Mater.* **2014**, *3*, 642.
[4] R. C. Webb, A. P. Bonifas, A. Behnaz, Y. Zhang, K. J. Yu, H. Cheng, M. Shi, Z. Bian, Z. Liu, Y.-S. Kim, W.-H. Yeo, J. S. Park, J. Song, Y. Li, Y. Huang, A. M. Gorbach, J. A. Rogers, *Nat. Mater.* **2013**, *12*, 938.
[5] S. Wang, M. Li, J. Wu, D.-H. Kim, N. Lu, Y. Su, Z. Kang, Y. Huang, J. A. Rogers, *J. Appl. Mech. Trans. ASME* **2012**, 79.
[6] D.-H. Kim, Y.-S. Kim, J. Wu, Z. Liu, J. Song, H.-S. Kim, Y. Y. Huang, K.-C. Hwang, J. A. Rogers, *Adv. Mater.* **2009**, *21*, 3703.
[7] J. Lee, J. Wu, M. Shi, J. Yoon, S.-I. Park, M. Li, Z. Liu, Y. Huang, J. A. Rogers, *Adv. Mater.* **2011**, *23*, 986.
[8] J. Wu, M. Li, W.-Q. Chen, D.-H. Kim, Y.-S. Kim, Y.-G. Huang, K.-C. Hwang, Z. Kang, J. A. Rogers, *Acta Mech. Sin.* **2010**, *26*, 881.
[9] A. Kaneko, N. Asai, T. Kanda, *J. Hand Therapy* **2005**, *18*, 421.
[10] E. S. Dellon, R. Mourey, A. L. Dellon, *Plastic Reconstructive Surg.* **1992**, *90*, 112.
[11] K.-I. Jang, H. U. Chung, S. Xu, C. H. Lee, H. Luan, J. Jeong, H. Cheng, G.-T. Kim, S. Y. Han, J. W. Lee, J. Kim, M. Cho, F. Miao, Y. Yang, H. Na. Jung, M. Flavin, H. Liu, G. W. Kong, K. J. Yu, S. I. Rhee, J. Chung, B. Kim, J. W. Kwak, M. H. Yun, J. Y. Kim, Y. M. Song, Y. Paik, Y. Zhang, Y. Huang, J. A. Rogers, *Nat. Commun.* **2015**, *6*, 6566.
[12] *ABAQUS Analysis User's Manual*, **2010**, V6.10.